Electronic Supplementary Material (ESI) for Chemical Communications.

Supporting Information

A self-quenching fluorescence probe-mediated exponential isothermal amplification system for highly sensitive and specific detection of microRNAs

Jun Zhao,[a] Jiandong Wu,[d] Xiaosong Wu,[ab] Guoqing Deng,[a] Yong Liu,[a] Francis Lin[c]* and Ling Zhu[a]*

[a] *Center of Engineering Technology Research for Biomedical Optical Instrument, Hefei Institutes of Physical Science, Chinese Academy of Sciences, Hefei 230031, P.R. China*

[b] *University of Science and Technology of China, Hefei 230026, P.R. China*

[c] *Department of Physics and Astronomy, University of Manitoba, Winnipeg R3T2N2, Canada*

[d] *Bionic Sensing and Intelligence Center, Institute of Biomedical and Health Engineering, Shenzhen Institutes of Advanced Technology, Chinese Academy of Sciences, Shenzhen 518055, P.R. China*

** Corresponding authors. E-mail addresses: Francis.Lin@umanitoba.ca (Francis Lin) and zhul@aiofm.ac.cn (Ling Zhu)*

Table of Contents

1. Experimental section

1.1 Materials and apparatus

All oligonucleotides (Table S1) were synthesized and purified by HPLC from Sangon Biotech Co., Ltd. (Shanghai, China). Vent (exo$^-$) DNA polymerase and Nt.BstNBI nicking enzyme were purchased from New England Biolabs (Beverly, USA). Mir-X miRNA First-Strand Synthesis Kit, TB Green Advantage qPCR Premix Kit, dNTP mixture (dNTPs), EASY dilution buffer, and RNase-free water were purchased from Takara Biomedical Technology Co., Ltd. (Dalian, China). The blood samples were collected from the First Affiliated Hospital of University of Science and Technology of China (Hefei, China), and all participants involved had signed the written informed consents prior to sampling. Meanwhile, this clinical research had been approved by the Ethics Committee of the First Affiliated Hospital of USTC (Ethical No. 2019KY66). Real-time SqPIA assays were carried out on the Roche Light Cycler 480 system (Basel, Switzerland). The assays on the background fluorescence intensity of probes were performed on the Roche Light Cycler 96 system (Basel, Switzerland). Tanon-2500 imaging system (Shanghai, China) was used for agarose electrophoresis analysis.

Table S1. Sequences of oligonucleotide* used in this research.

Name	Sequence (5′ to 3′)
miR-21	UAGCUUAUCAGACUGAUGUUGA
miR-27a	UUCACAGUGGCUAAGUUCCGC
miR-223	UGUCAGUUUGUCAAAUACCCCA
miR-223-5p	CGUGUAUUUGACAAGCUGAGUU
miR-599	GUUGUGUCAGUUUAUCAAAC
miR-223-Mut1	UGUCAGUUUGUCGAAUACCCCA
miR-223-Mut2	UGUCAGUUUGGCGAAUACCCCA
miR-223-Mut3	UGUCAGUUUGGCGAAUACACCA
mProbe-QG-21	CCCGTGGAGTCTGT-(BHQ1)GT-(FAM)TCAACATCAG
hairpin probe-21	BHQ1-ATTGGCTCTGGTGCAGGGTCCGAGGTATTCGCACCAGAGCCAAT-(FAM)AAAGAGTCTGTGTAGCTTATCAG
mProbe-QG -27a	CGCCTCGAGTCGTT-(BHQ1)GT-(HEX)GCGGAACTTA
hairpin probe-27a	BHQ1-ATTGGCTCTGGTGCAGGGTCCGAGGTATTCGCACCAGAGCCAAT-(HEX)AAAGAGTCCTATTTCACAGTGG
mProbe-QG -223	CCCGTGGAGTCGTT-(BHQ2)GT-(ROX)TGGGGTATTT
hairpin probe-223	BHQ2-ATTGGCTCTGGTGCAGGGTCCGAGGTATTCGCACCAGAGCCAAT-(ROX)AAAGAGTCGTATTGTCAGTTTGT
PCR-miR-21-F	AACACGCTAGCTTATCAGACTGATG
PCR-miR-27a-F	AACAAGTTCACAGTGGCTAAGTTCC
PCR-miR-223-F	AACACGCTGTCAGTTTGTCAAATAC
PCR-universal-R	CAGTGCAGGGTCCGAGGT
RT primer	CAGTGCAGGGTCCGAGGTCAGAGCCACCTGGGCAATTTTTTTTTTTVN
UR-miR-21	FAM-TAGCTTATCAGACTGATGTTGA
SP-miR-21	TCAACATCAGTCTGATAAGCTACCCTTACATCGTGGGTGCTTCCGTAAGGGTGGGAGGGAGGGAGGGAGAG

* The base difference between miR-223 and its homologous sequences are underlined.

1.2 Standard procedures of miRNA detection in SqPIA system

All oligonucleotides were diluted into 10 μM stock solutions using RNase-free water. Components of reaction mixtures mainly contain 1.25×10^{-1} μM probes, 1 × NEBuffer 3 (100 mM NaCl, 50 mM Tris-HCl (pH 7.9), 10 mM $MgCl_2$, 1 mM dithiothreitol), 1 μL of dNTPs (10 mM), 1 μL of Vent (exo^-) DNA polymerase (2 U/μL), 0.4 μL of Nt.BstNBI (10 U/μL). And, a certain concentration of targeted miRNA was added into this reaction system according to experimental necessities. Finally, an appropriate amount of water was replenished to the total volume of 20 μL. The reaction was incubated at 55℃ throughout, and the signal acquisition was performed at every 60 s. All tests were repeated three independent times, and the group without targeted miRNA was set up as negative control, simultaneously.

1.3 Agarose electrophoresis analysis

To check the specificity of SqPIA system in miRNA detection, the products of the amplification reaction were analyzed through 2% of agarose gel, and electrophoresis assay was subsequently analyzed in 1 × TBE buffer at 120 V constant voltage for 35 min. Finally, the gel was photographed using Tanon-2500 imaging system (Shanghai, China).

1.4 Real sample analysis

The blood samples from hepatocellular carcinoma (HCC) patients and healthy donors were collected for serum separation and total RNA extraction, and the process of extraction was referred to TRIzol LS (Thermo Scientific, Waltham, USA) manual.[1] To evaluate the quantitative accuracy of the SqPIA method, the purified total RNAs was evenly divided into two equal portions: one part of sample as the direct target used for miRNA quantification utilizing the SqPIA strategy, and the other one as the indirect target which was firstly reverse transcribed into cDNA, and then performed to quantify miRNAs using RT-qPCR.

2. Supplementary figures

2.1 Comparison of the background fluorescence intensity between mProbe-QG and reported probes

To further evaluate the performance of mProbe-QG in the self-quenching of fluorescence, the comparison of the background fluorescence intensity between the mProbe-QG and a reported self-assembled probe (SP-UR)[2, 3] was performed. It should be pointed out that the SP-UR is composed of a hairpin structure (SP) strand and a universal reporter (UR) strand. Thereinto, the SP strand has a rich region of G-base in its stem, while the 5′ end of the UR strand was labeled with a reporter. Both the reporter and the G-base are spatially close to each other, thus can decrease the background fluorescence of the SP-UR. Thus, based on the principle stated above, the sequences of UR-miR-21 (Table S1) and SP-miR-21 (Table S1) employed in this assay were synthesized and tested. The difference of background fluorescence intensity between the mProbe-QG and the SP-UR was shown in Fig. S1A, a highly significant difference was obtained in the background fluorescence intensity under the same conditions. Hence, we can conclude that the proposed mProbe-QG has better performance in the self-quenching of fluorescence than reported SP-UR.

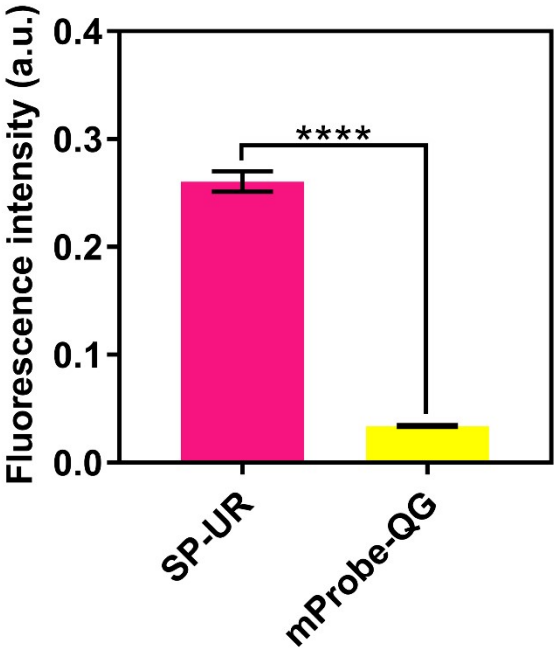

Fig. S1 Comparison of the background fluorescence intensity between the proposed mProbe-QG and the reported SP-UR. Error bars represented the SD of three independent replicates. Statistical significance was calculated using *t*-tests, ****: $p < 0.0001$.

2.2 Structural illustration of hairpin probe used in SqPIA system

It is well known that secondary amplification is an important prerequisite for exponential amplification, and an effective way to solve non-specific amplification.[4] To achieve the goals on exponential amplification of products and exponential growth of signals, a hairpin probe (HPP) with the same self-quenching feature was also designed, as shown in Fig. S2. The 5′ end of HPP was labeled by the quencher, and the base at the 3′ end of the stem region was modified with the reporter. Thus, the signal of the fluorophore could be blocked by the quencher. Besides, a special structure contained an extended single strand for binding and a same restriction site for nicking were also designed. Finally, the HPP, as well as the mProbe-QG stated above was employed in the SqPIA system for miRNA detection.

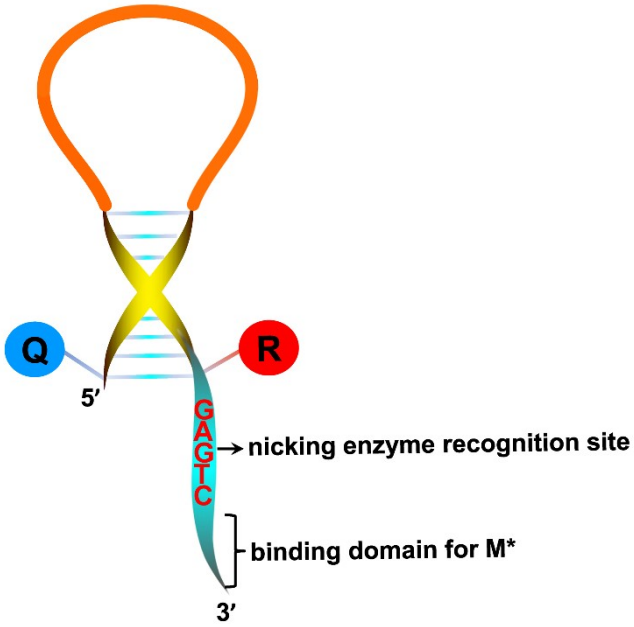

Fig. S2 Structure diagram of the hairpin probe.

2.3 Validation of the amplification products using agarose gel electrophoresis

To validate the specificity of the amplification products generated in the SqPIA system, the agarose gel electrophoresis assay was performed. And, two different amplification products should be theoretically obtained owing to the SqPIA system is composed of two cycles. It turned out, not too surprisingly, that two distinct bands which around 78 bp (product 1) and 38 bp (product 2) were both detected in test groups, as shown in Fig. S3 (lane A, lane B, and lane C). Thereinto, the product 2 was obtained by hybridization and extension of the targeted miRNA or the product M* with the mProbe-QG, and product 1 was the fragments amplified by the product M and the hairpin probe. By contrast, no obvious bands were visible in the negative controls (lane D, lane E, and lane F) which lack the targeted miRNA. Therefore, these results demonstrated that the constructed SqPIA system was capable of detecting targeted miRNAs with high specificity.

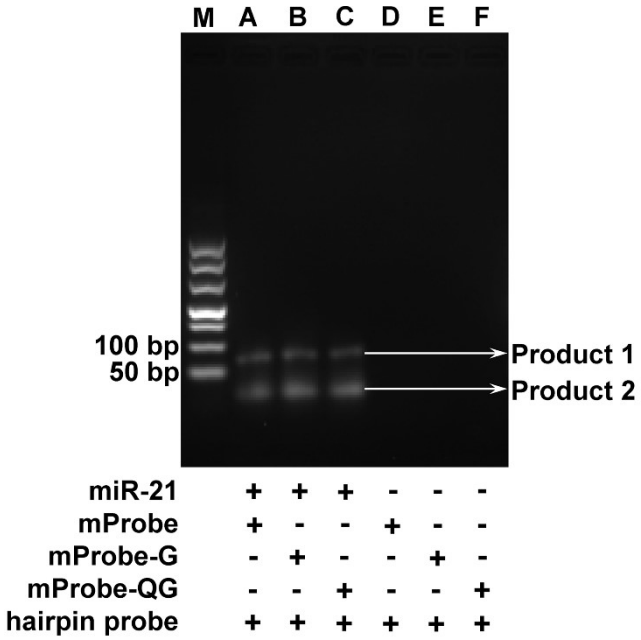

Fig. S3 Agarose gel electrophoresis analysis of amplification products of SqPIA method. (M): DL500 DNA marker. (A): 1.0 $\times 10^{-9}$ M miR-21 + 1.25 $\times 10^{-7}$ M HPP + 1.25 $\times 10^{-7}$ M mProbe. (B): 1.0 $\times 10^{-9}$ M miR-21 +1.25 $\times 10^{-7}$ M HPP + 1.25 $\times 10^{-7}$ M mProbe-G. (C): 1.0 $\times 10^{-9}$ M miR-21 + 1.25 $\times 10^{-7}$ M HPP + 1.25 $\times 10^{-7}$ M mProbe-QG. (D): 1.25 $\times 10^{-7}$ M HPP + 1.25 $\times 10^{-7}$ M mProbe. (E): 1.25 $\times 10^{-7}$ M HPP + 1.25 $\times 10^{-7}$ M mProbe-G. (F): 1.25 $\times 10^{-7}$ M HPP + 1.25 $\times 10^{-7}$ M mProbe-QG.

2.4 Improvements of signal-to-background ratio in SqPIA system

To investigate the efficacy of SqPIA system in improving signal-to-background ratio, we here employed quantitative real-time amplification assay to analyze the difference of signal changes before and after the reaction. Fig. S4A showed the real-time fluorescence plots drew from raw data of fluorescence intensity that had not been baseline corrected. It was pretty obvious that the initial background fluorescence intensity of SqPIA system which employing the mProbe-QG was significantly lower than that using the mProbe, and even lower than the mProbe-G group. This was definitely benefited from the role of an adjacent double-quencher, particularly to an additional usage of G base which possesses high-efficiency quenching.[5] So, it was indicated that the background fluorescence of the probe ultimately determined the initial fluorescence intensity of the reaction system. Correspondingly, normalized fluorescence plots were shown in Fig. S4B. It was not hard to see that the range of change in fluorescence intensity before and after SqPIA reaction utilizing mProbe-QG was significantly greater than that using mProbe, and it was, of course, applied to the mProbe-G. Hence, we can conclude that the usage of the mProbe-QG or mProbe-G that with lower background fluorescence would contribute to improving the signal-to-background ratio. In summary, the lower the background fluorescence of the probe was, the larger the signal changed, thus, the higher the detective signal-to-background ratio produced. And this would, in a sense, probably beneficial to detect low-abundance circulating miRNAs in clinical samples.

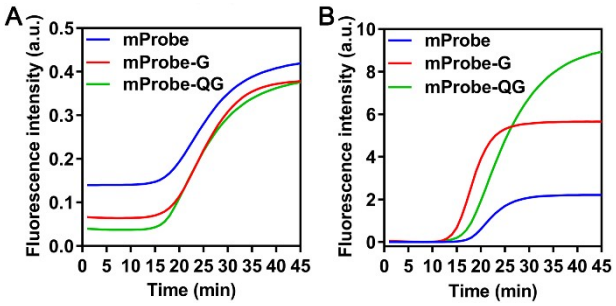

Fig. S4 Influence of probes with different background fluorescence to signal-to-background ratio. (A) Real-time curves depicted the changes of original fluorescence intensity without baseline correction. (B) Real-time curves depicted the changes of fitting fluorescence intensity under baseline correction.

2.5 Optimization of concentration of Vent (exo⁻) DNA polymerase in SqPIA system

DNA polymerase occupies great importance not only in the SqPIA system we constructed, but in other isothermal amplification as well. Sometimes, different concentrations of DNA polymerase would directly affect the amplification efficacy. Thus, effective amplification cannot be achieved if an unmatched concentration of the DNA polymerase is added into the reaction system. In this research, in order to determine the optimal concentration of Vent DNA polymerase, the final enzyme concentration of the SqPIA system within the scope of 0.01 U/μL to 0.1 U/μL was tested. As shown in Fig. S5, the poor trends of linear growth were found when the concentration of Vent between 0.01 U/μL and 0.02 U/μL (Fig. S5A and Fig. S5B), indicating that the amount of enzyme used was not enough for the effective response. By contrast, the fluorescence intensity of curves was considerably enhanced when the concentration of Vent continued rising, and clear "S"-shaped curves were merely obtained until at 0.1 U/μL (Fig. S5D). At this point, we can deem that the concentration of enzyme met the demand for an exponential growth of the amplified product. Therefore, the optimal concentration of Vent DNA polymerase in the SqPIA system is 0.1 U/μL.

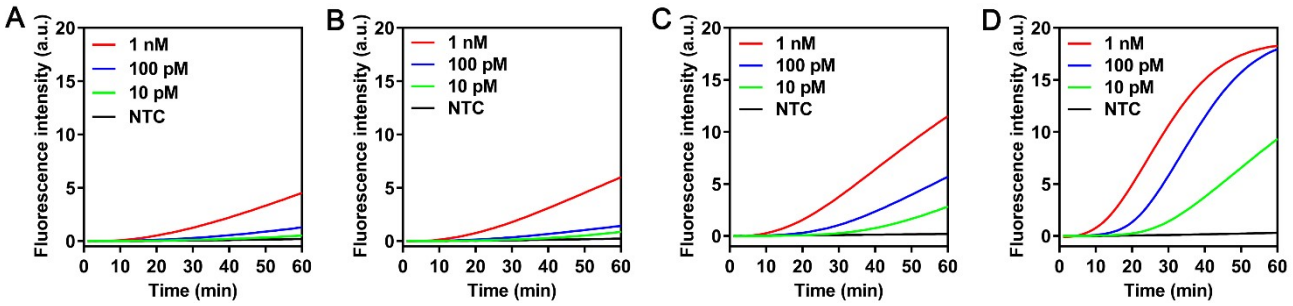

Fig. S5 Optimization of concentration of Vent (exo⁻) DNA polymerase in SqPIA system. Real-time fluorescence curves were produced by 1 nM, 100 pM, and 10 pM miR-223, and the group without miR-223 was set as a negative control simultaneously. The concentration of Vent (exo⁻) DNA polymerase was (A) 0.01 U/μL, (B) 0.02 U/μL, (C) 0.05 U/μL and (D) 0.1 U/μL, respectively.

2.6 Optimization of concentration of Nt.BstNBI nicking enzyme in SqPIA system

In this study, the role played by Nt.BstNBI nicking enzyme is also important apart from the Vent DNA polymerase stated above. Thus, to seek the optimal concentration of the Nt.BstNBI, the SqPIA system with a final concentration within the scope of 0.1 U/μL to 0.5 U/μL was tested. As shown in Fig. S6, the linear uniformity was poor when Nt.BstNBI was 0.1 U/μL in the reaction system (Fig. S6A). And, a great linear uniformity was followed obtained when the concentration of Nt.BstNBI reached 0.2 U/μL (Fig. S6B). However, the signal caused by nonspecific amplification was significantly increased as soon as the concentration of Nt.BstNBI reached 0.5 U/μL (Fig. S6C). To our knowledge, a higher concentration of nicking enzyme in the reaction system can sometimes change its specificity, so-called star activity.[6] Therefore, the optimal concentration of Nt.BstNBI nicking enzyme in the SqPIA system is 0.2 U/μL.

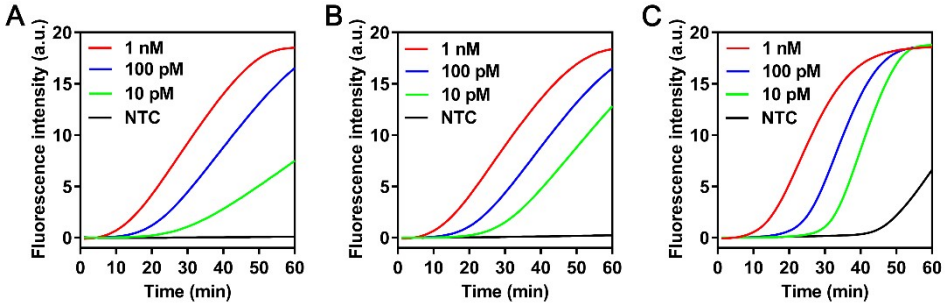

Fig. S6 Optimization of concentration of Nt.BstNBI nicking enzyme in SqPIA system. Real-time fluorescence curves were produced by 1 nM, 100 pM, and 10 pM miR-223, and the group without miR-223 was set as a negative control simultaneously. The concentration of Nt.BstNBI nicking enzyme was (A) 0.1 U/μL, (B) 0.2 U/μL and (C) 0.5 U/μL, respectively.

2.7 Optimization of reaction temperature in SqPIA system

The reaction temperature of isothermal amplification is largely determined by the enzymes. In this study, Vent DNA polymerase and Nt.BstNBI are the two enzymes involved in the SqPIA reaction. Thereinto, the enzyme activity of Nt.BstNBI can reach the maximum when the temperature is around 55 °C. However, the working temperature range of the Vent DNA polymerase is very wide. So, to determine the optimal reaction temperature, the same reaction system was respectively tested at 52 °C, 55 °C, and 58 °C. As shown in Fig. S7, the reaction was completely suppressed when the working temperature was too low (Fig. S7A) or too high (Fig. S7C). And only when the reaction was incubated at 55 °C, can better amplification results be obtained (Fig. S7B). Hence, we can conclude that the optimal reaction temperature is 55 °C.

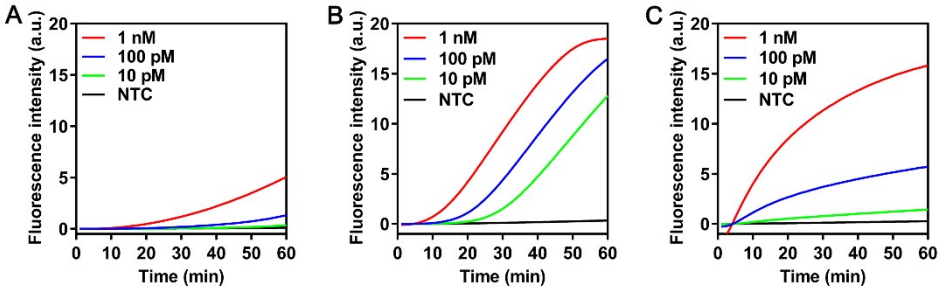

Fig. S7 Optimization of reaction temperature in SqPIA system. Real-time fluorescence curves were produced by 1 nM, 100 pM, 10 pM miR-223, and the group without miR-223 was set as a negative control simultaneously. The reaction temperature was (A) 52 °C, (B) 55 °C and (C) 58 °C, respectively.

2.8 Optimization of probe concentration in SqPIA system

The strategy proposed in this study is quite different from the majority of previous methods, this is principally because the probes used in SqPIA system have completely replaced the roles of primers. In other words, the probes can not only act directly on targeted miRNA, but also emit fluorescent signal. Thus, in order to determine the optimal concentration of probes, a final concentration of reaction from 0.05 μM to 0.5 μM were tested. As shown in Fig. S8, the fluorescence intensity in the plateau of the curve was significantly lower than other test groups if with the lower concentration of probes (Fig. S8A). When the concentration of probes reached 0.125 μM, clear "S"-shaped curves appeared, and a higher fluorescence intensity was obtained (Fig. S8B). However, with the increasing of probe concentration, the final fluorescence intensity cannot rise anymore (Fig. S8C and Fig. S8D). To sum up, we can demonstrate that the optimal concentration of probes is 0.125 μM.

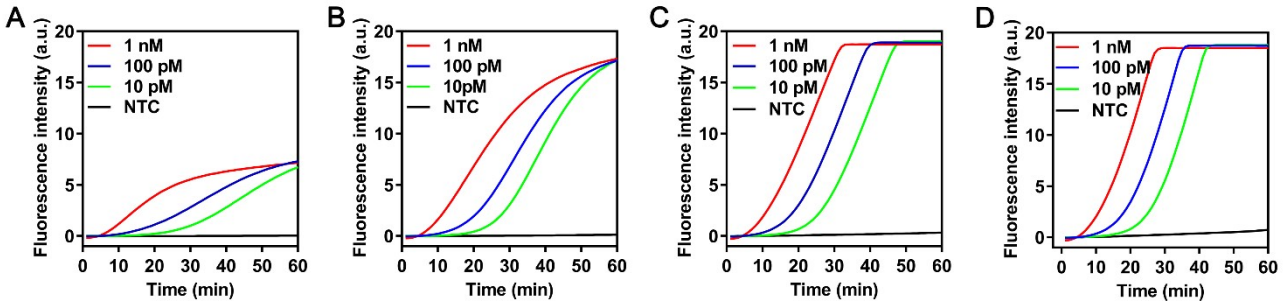

Fig. S8 Optimization of probe concentration in SqPIA system. Real-time fluorescence curves were produced by 1 nM, 100 pM, and 10 pM miR-223, and the group without miR-223 was set as a negative control simultaneously. The probe concentration was (A) 0.05 μM, (B) 0.125 μM, (C) 0.25 μM and (D) 0.5 μM, respectively.

2.9 Influence of temperature to secondary structure of oligonucleotide

The SqPIA strategy proposed in this study, and other isothermal amplification methods are both the techniques that amplify at a constant temperature. As lack of the denaturation process at the high temperature, so the secondary structure of probe or miRNA sequence might affect the efficiency of the hybridization between them. Hence, the NUPACK tool (http://www.nupack.org/)[7] was used for analyzing the secondary structure of oligonucleotides at different temperatures. As shown in Fig. S9, The sequence of miR-21 can hybridize in itself at 37 °C (Fig. S9A), thus, the reduction in binding area of sequence would result in a significant decrease in reaction efficiency of SqPIA. However, this hybridized structure disappeared and a linear structure formed when the temperature rose to 56 °C (Fig. S9C). Similarly, for the probe (mProbe-QG-21) used in the study was no exception, it was also hybridized at 37 °C (Fig. S9D), but presented in linear at a higher temperature (Fig. S9E and Fig. S9F). Without a doubt, the binding efficiency between miRNA (Fig. S9C) and probe (Fig. S9F) in the linear state could definitely be higher than them in the hybridized state (Fig. S9A or Fig. S9C). More importantly, the probability of the effective collision of active molecules can be significantly increased at 55 °C, when compared to a lower reaction temperature (37 °C or 42 °C), so that it would further improve the reaction efficiency. In a word, the reaction temperature determines the secondary structure of oligonucleotide, and then directly affect the detective efficiency in the SqPIA, as well as other isothermal amplification methods. Therefore, a higher reaction temperature (55 °C) was preferred in this study.

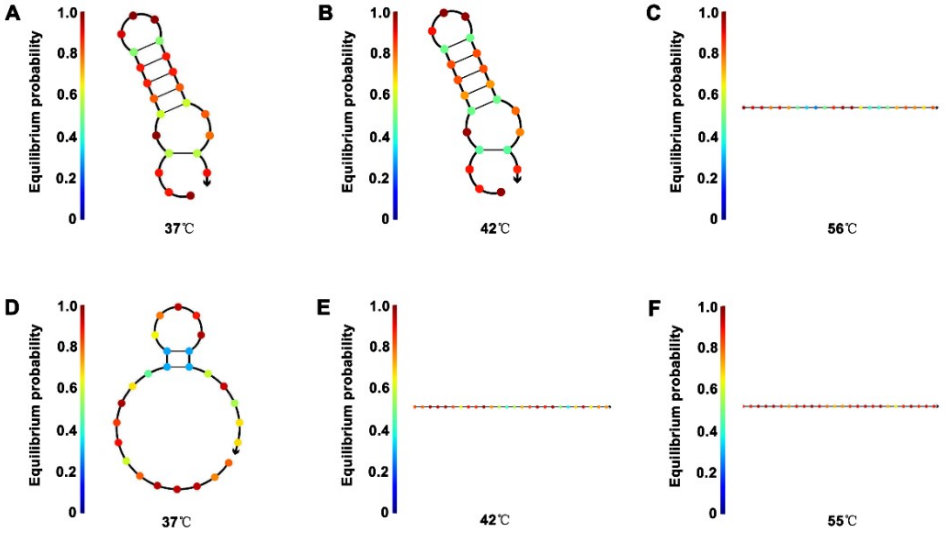

Fig. S9 Influence of temperature on secondary structure of oligonucleotide. The secondary structure of miR-21 sequence at (A) 37 °C, (B) 42 °C, and (C) 56 °C, respectively. The secondary structure of mProbe-QG-21 sequence at (D) 37 °C, (E) 42 °C, and (F) 55 °C, respectively.

2.10 Analytical performance of multiplexed detection of miRNAs

To evaluate the analytical performance of SqPIA system in multiplexed detection of miRNAs, three miRNAs were tested simultaneously in the same reaction system, as shown in Fig. S10A. Among them, the red curves represented the detection results of miR-21 using the probes (mProbe-QG-21 and hairpin probe-21) labeled with FAM fluorophore. Similarly, the green curves and the blue curves corresponded to the miR-27a labeled with HEX fluorophore and the miR-223 labeled with ROX fluorophore, respectively. It was not difficult to see that good homogeneity was displayed not only in miR-21 test group, but also in miR-27a and miR-223 group. Obviously, these could be further validated through an ideal linear relationship ($R^2 > 0.9$) between the POI values and logarithmic values of the dilution ratio (Fig. S10B, Fig. S10C, and Fig. S10D). Therefore, it suggested that the self-quenching fluorescence probes-mediated exponential amplification system was well-equipped to achieve multiplexed detection of miRNAs in a single reaction system. Without a doubt, this will be of immense significance for improving the detective accuracy of circulating miRNA biomarkers in clinical.

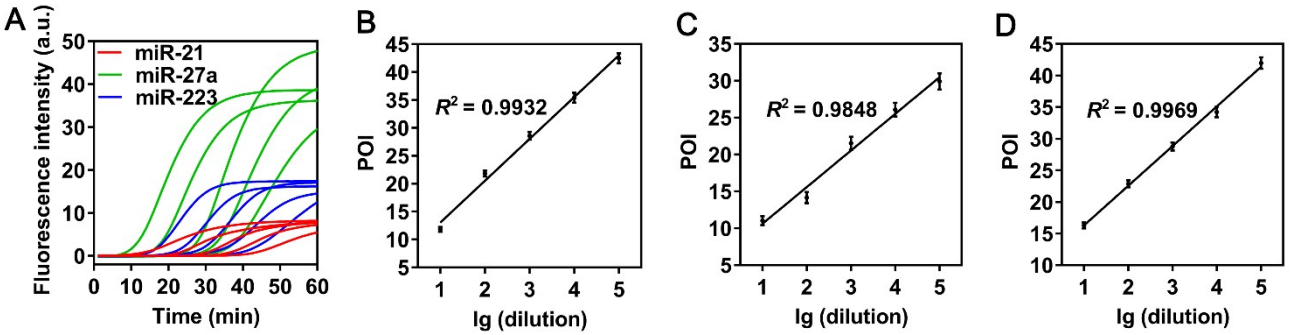

Fig. S10 Analysis of triplex detection of miRNAs in SqPIA system. (A) Real-time fluorescence curves with same color represented the detection results of miRNA target with tenfold concentration difference. (B) Linear relationship between POI values and dilution of miR-21. (C) Linear relationship between POI values and dilution of miR-27a. (D) Linear relationship between POI values and dilution of miR-223. Error bars represented the SD of three independent replicates.

2.11 Analysis of the availability of selected probes in SqPIA system

To ensure high efficiency of SqPIA system in miRNA quantification, the probes used for quantifying the miRNA markers (miR-21, miR-27a, and miR-223) were tested and optimized, as shown in Fig. S11. It was not difficult to see the generated amplification curves which corresponded to different concentrations of miRNA template showed good homogeneity. Furthermore, a high linear correlation ($R^2 > 0.99$) was all observed between POI values and negative logarithmic values in the three assays. Hence, we can conclude that the probes employed in the SqPIA system were suitable for the quantification of miRNA markers.

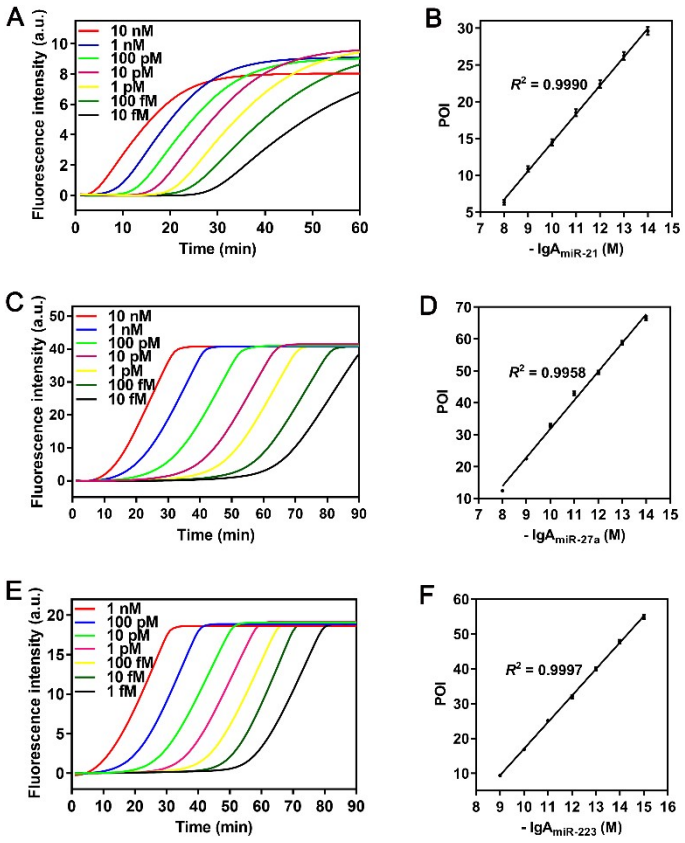

Fig. S11 Analysis of the availability of selected probes in SqPIA system. (A) Real-time fluorescence curves of quantification of miR-21with different concentrations within the scope of 10 fM to 10 nM. (B) Linear relationship between POI values and negative logarithmic values of concentration for miR-21. (C) Real-time fluorescence curves of quantification of miR-27a with different concentrations within the scope of 10 fM to 10 nM. (D) Linear relationship between POI values and negative logarithmic values of concentration for miR-27a. (E) Real-time fluorescence curves of quantification of miR-223 with different concentrations within the scope of 1 fM to 1 nM. (F) Linear relationship between POI values and negative logarithmic values of concentration to miR-223. Error bars represented the SD of three independent replicates.

2.12 Analysis of the availability of selected primers in RT-qPCR system

In this study, RT-qPCR was employed for evaluating the quantitative accuracy of the proposed SqPIA method. Similarly, in order to ensure the high efficiency of RT-qPCR system in miRNA quantification, the primers used for quantifying the miRNA markers (miR-21, miR-27a, and miR-223) were also tested and optimized, as shown in Fig. S12. It was obvious that a good homogeneity was obtained in the amplification curves corresponded to different concentrations of miRNA template. Besides, a high linear correlation (R^2 > 0.99) was all observed between *Cq* values and negative logarithmic values in three assays. Hence, we can conclude that the primers employed in the RT-qPCR system were suitable for the quantification of miRNA markers.

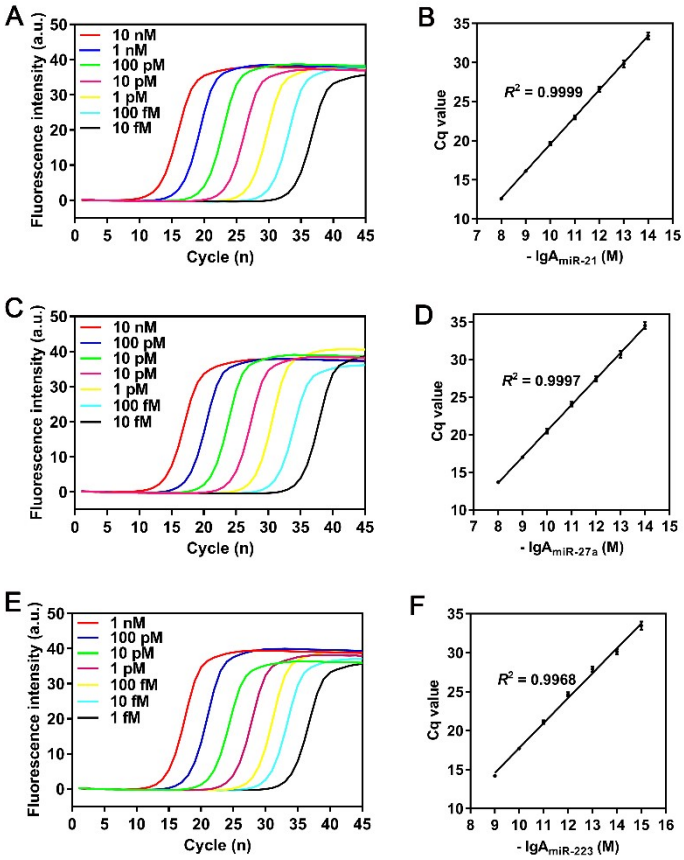

Fig. S12 Analysis of the availability of selected primers in RT-qPCR system. (A) Real-time fluorescence curves of quantification of miR-21 with different concentrations within the scope of 10 fM to 10 nM. (B) Linear relationship between *Cq* values and negative logarithmic values of concentration for miR-21. (C) Real-time fluorescence curves of quantification of miR-27a with different concentrations within the scope of 10 fM to 10 nM. (D) Linear relationship between *Cq* values and negative logarithmic values of concentration for miR-27a. (E) Real-time fluorescence curves of quantification of miR-223 with different concentrations within the scope of 1 fM to 1 nM. (F) Linear relationship between *Cq* values and negative logarithmic values of concentration for miR-223. Error bars represented the SD of three independent replicates

2.13 Analytical performance in real sample quantification

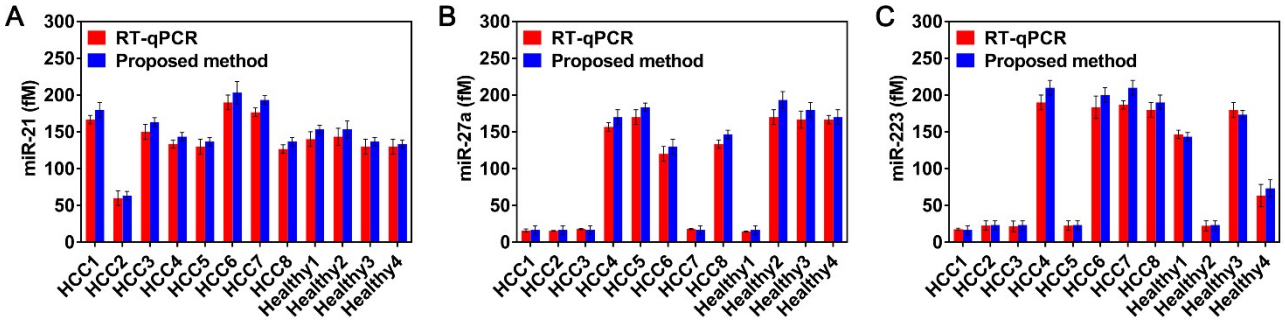

Fig. S13 Quantification of serum miRNAs of HCC patients and healthy using RT-qPCR (red) and proposed method (blue). Error bars represented the SD of three independent replicates. (A) miR-21. (B) miR-27a. (C) miR-223.

3. Supplementary table

Table S2. Comparisons of isothermal amplification-mediated approach for multiplexed detection of miRNAs.

Technique	Time	Detection range (M)	LOD (M)	Multiplexed	Step	Reference
RCA-mediated	> 2 h	10^{-13} - 10^{-11}	5.0×10^{-14}	Yes	Single step	[8]
RCA/SDA-mediated	> 4 h	10^{-15} - 10^{-11}	5.0×10^{-16}	Yes	Mult-step	[9]
SDA-mediated	> 90 min	10^{-15} - 10^{-11}	4.0×10^{-16}	Yes	Single step	[10]
EXPAR-mediated	163 min	10^{-12} - 10^{-7}	2.0×10^{-16}	Yes	Mult-step	[11]
TMSD-mediated	> 2 h	10^{-14} - 10^{-10}	5.8×10^{-15}	Yes	Mult-step	[12]
CHA-mediated	3 h	10^{-12} - 10^{-10}	1.8×10^{-12}	Yes	Single step	[13]
CRISPR-mediated	60 min	10^{-13} - 10^{-10}	1.26×10^{-16}	Yes	Mult-step	[14]
RCA-mediated	16 h	10^{-11} - 10^{-9}	1.09×10^{-12}	Yes	Mult-step	[15]
HCR-mediated	> 4 h	10^{-9} - 10^{-6}	1.0×10^{-9}	Yes	Mult-step	[16]
RCA-mediated	< 1 h	10^{-14} - 10^{-11}	4.9×10^{-15}	Yes	Mult-step	[17]
SqPIA	< 90 min	10^{-17} - 10^{-9}	0.8×10^{-18}	Yes	Single step	Our approach

4. Reference

1 A. B. Hummon, S. R. Lim, M. J. Difilippantonio and T. Ried, *Biotechniques*, 2007, **42**, 467-472.

2 L. M. Huang, G. H. Aryal, S. W. Tam-Chang, N. G. Publicover and K. Hunter, *Analyst*, 2016, **141**, 1376-1382.

3 S. W. Tam-Chang, T. D. Carson, L. M. Huang, N. G. Publicover and K.W. Hunter, *Anal. Biochem.*, 2007, **366**, 126-130.

4 J. Qian, S. A. Boswell, C. Chidley, Z. X. Lu, M. E. Pettit, B. L. Gaudio, J. M. Fajnzylber, R. T. Ingram, R. H. Ward and J. Z. Li, *Nat. Commun.*, 2020, **11**, 1-10.

5 H. H. Mao, G. H. Luo, Y. X. Zhan, J. Zhang, S. Yao and Y. Yu, *Analyst*, 2018, **143**, 3292-3301.

6 H. Wei, C. Therrien, A. Blanchard, S. X. Guan and Z. Y. Zhu, *Nucleic Acids Res.*, 2008, **36**, e50.

7 J. N. Zadeh, C. D. Steenberg, J. S. Bois, B. R. Wolfe, M. B. Pierce, A. R. Khan, R. M. Dirks and N. A. Pierce, *J. Comput. Chem.*, 2011, **32**, 170-173.

8 K. Treerattrakoon, T. Jiemsakul, C. Tansarawiput, P. Pinpradup, T. Iempridee, P. Luksirikul, K. Khoothiam, T. Dharakul and D. Japrung, *Anal. Biochem.*, 2019, **577**, 89-97.

9 S. Q. Liu, H. Fang, C. J. Sun, N. N. Wang and J. Li, *Analyst*, 2018, **143**, 5137-5144.

10 X. J. Qu, H. J. Jin, Y. Q. Liu and Q. J. Sun, *Anal. Chem.*, 2018, **90**, 3482-3489.

11 W. C. Zhang, F. Hu, Q. Zhang, J. Q. Zhang, Y. B. Mao, P. Wang and Y. Q. Gu, *Talanta*, 2018, **179**, 685-692.

12 S. Z. Yue, T. T. Zhao, S. Bi and Z. P. Zhang, *Biosens. Bioelectron.*, 2017, **98**, 234-239.

13 J. Y. Xu, J. J. Guo, N. Golob-Schwarzl, J. Haybaeck, X. Qiu and N. Hildebrandt, *ACS Sensors*, 2020, **5**, 1768-1776.

14 J. J. Li, S. S. Yang, C. Zuo, L. Dai, Y. C. Guo and G. M. Xie, *ACS Sensors*, 2020, **5**, 970-977.

15 Z. A. Hu, F. J. Xu, G. W. Sun, S. C. Zhang and X. R. Zhang, *Chem. Commun.*, 2020, **56**, 5409-5412.

16 X. W. Wei, F. K. Bian, X. X. Cai, Y. Wang, L. J. Cai, J. Yang, Y. F. Zhu and Y. J. Zhao, *Anal. Chem.*, 2020, **92**, 6121-6127.

17 M. Kim, D. M. Kim and D. E. Kim, *Analyst*, 2020, **145**, 6130-6137.